
Article:
Bai, L, Zhang, L, Guo, J et al. (2016) Evaporation/boiling heat transfer characteristics in an artery porous structure. Applied Thermal Engineering, 104. pp. 587-595. ISSN: 1359-4311

https://doi.org/10.1016/j.applthermaleng.2016.05.113

Experimental study on the supercritical startup of cryogenic loop heat pipes with redundancy design

Yuandong Guo[1], Guiping Lin[1], Lizhan Bai[1,3,*], Xueqin Bu[1],
Hongxing Zhang[2], Jiang He[2], Jianyin Miao[2], Dongsheng Wen[3]

1 Laboratory of Fundamental Science on Ergonomics and Environmental Control, School of Aeronautic Science and Engineering, Beihang University, Beijing 100191, PR China

2 Beijing Key Laboratory of Space Thermal Control Technology, Beijing Institute of Spacecraft System Engineering, China Academy of Space Technology, Beijing 100094, PR China

3 School of Chemical and Process Engineering, University of Leeds, Leeds, LS2 9JT, UK

Abstract: Cryogenic loop heat pipe (CLHP) is one of the key components in the future space infrared exploration system, which enables effective and efficient cryogenic heat transport over a long distance with a flexible thermal link. To realize reliable and long life operation, a CLHP-based thermal control system with redundancy design was proposed in this work, where two nitrogen-charged CLHPs were employed to provide cryocooling at 80-100K. This study focused on the supercritical startup of the CLHPs with redundancy design, and an extensive experimental study under four possible working modes was conducted. Experimental results showed that with 2.5W applied to the secondary evaporator, each CLHP could realize the supercritical startup successfully in the normal working mode; however, the required time differed a lot because the difference in the transport line diameter significantly affected the cryocooling capacity to the primary evaporator. In the backup conversion mode, instant switch of the two primary evaporators may cause an operation failure, and an auxiliary operation of the secondary evaporator in advance was necessary to make the primary liquid line filled with liquid. In the malfunction conversion mode, the simulated infrared detector had to be first shut down, but the time needed for the backup CLHP to realize the supercritical startup became obviously shorter than that in the normal working mode, because the primary evaporator of the backup CLHP was always in a cryogenic state. In the dual operation mode, the two CLHPs could realize the supercritical startup simultaneously, but a temperature oscillation phenomenon was observed, which can be eliminated by increasing the heat load applied to the secondary evaporator.

Keywords: loop heat pipe; cryogenic; supercritical startup; working mode; experiment

* Corresponding author. Tel.: +86 10 8233 8600; Fax: +86 10 8233 8600.
E-mail address: bailizhan@buaa.edu.cn (L. Bai).

1 Introduction

Heat pipe is an advanced two-phase heat transfer device, which combines the principles of both thermal conduction and liquid/vapor phase change to efficiently manage the heat transfer processes between two solid interfaces, and its operating principle, performance and characteristics were detailed in Refs.[1, 2]. Since the first basic concept of heat pipe was proposed by Gaugler [3], it has attracted the interests of researchers worldwide, and various types of heat pipes operating at different temperature ranges have been developed to satisfy specific application requirements [4-7]. So far, heat pipes have been applied in a variety of areas in both space and terrestrial surroundings such as in the building natural ventilation system, electronics cooling, industrial waste heat recovery and spacecraft thermal control [8-13].

As one of the latest developments of the heat pipe technology, cryogenic loop heat pipe (CLHP) can realize efficient heat transport at the cryogenic temperatures. Depending on the working fluids charged, CLHPs can operate in a specific low temperature range, i.e., propane for the operating temperature range of 200-240 K, oxygen for 90-140 K, nitrogen for 80-110 K, neon for 30-40 K and hydrogen for 20-30 K, and when helium is selected as the working fluid, the operating temperature can be reached as low as 2-4 K. Compared with traditional cryogenic heat pipes, CLHP exhibits a variety of advantages such as higher heat transfer capacity, longer heat transport distance and stronger antigravity capability, as well as good flexibility for complex structures. An important example for the CLHP applications is in the thermal control of the space infrared exploration system where the infrared sensors/detectors have to be maintained at 80-100 K or even lower temperatures [14, 15].

For ambient loop heat pipe, the working fluids charged are typically ammonia, acetone, water, etc., which are in the two-phase state at ambient temperature. Because the evaporator wick is always saturated by the liquid through the matching design of the compensation chamber volume and the working fluid inventory, heat load can be applied to the evaporator immediately to initiate the startup. However, for CLHP, the situation becomes much

different. Because the critical temperatures of the cryogenic working fluids are much lower than the ambient temperature, i.e., the critical temperature of nitrogen is about 126 K, and the cryogenic working fluids are in the supercritical state at ambient temperature. In order to start up the CLHP, prior to the application of heat load to the evaporator, the working fluid inside must be first cooled to below its critical temperature until it condenses and saturates the evaporator wick, and an auxiliary measure will be needed to help realize the liquid saturation of the evaporator wick [16]. From the above analysis, a CLHP will inevitably experience a supercritical startup to realize the normal operation.

So far, several types of CLHPs employing different auxiliary measures to realize the supercritical startup have been developed, such as the gravity-assisted method [16], the secondary evaporator method [17-22], the auxiliary loop method [23-28] and the capillary pump method [29-30], as reviewed in our previous paper [31]. Because the CLHP employing the auxiliary loop method can realize the supercritical startup in space microgravity environment, and can manage the parasitic heat load effectively with a relatively high heat transport capacity, it is the most suitable for space applications and is selected as the object of study in this work. Below provides a brief review on the development of this type of CLHP.

James et al. [23] proposed an ethane-charged CLHP operating at a temperature range of 215-218K for passive optical bench cooling applications. Experimental results showed that the CLHP could reliably realize the supercritical startup from an initially supercritical temperature of 335K with a heat load of 60W applied to the secondary evaporator,. With a heat load of 5W applied to the secondary evaporator to manage the parasitic heat load, the CLHP achieved a 50W heat transport capability at 215K. Hoang et al. [14] developed a nitrogen-charged CLHP operating in a temperature range of 80-110K for across-gimbal cryocooling, which could successfully realize the supercritical startup from an initially supercritical temperature of 298K, with a heat load of 5W applied to the secondary evaporator. The maximum heat transport capability was determined to be 5W over a transport

distance of 4.3m. Later, a hydrogen-charged CLHP with a swing volume design was experimentally studied to reduce the system volume/weight. The CLHP could realize the supercritical startup with a heat load of 2.5W applied to the secondary evaporator when the shroud temperature was 200K; however, a supercritical startup failure occurred in a 298K environment due to large parasitic heat load. The CLHP could operate at a temperature range of 20-30K, and a maximum heat transport capability of 10W over a transport distance of 2.5m was obtained with a 80K shroud [15]. To solve important problems in cryogenic integration, Bugby et al. [24, 25] developed three CLHPs: an across-gimbal CLHP, a short and a long transport length miniaturized CLHP. The across-gimbal CLHP employed nitrogen as the working fluid with a heat transport range of 2-20W. Both the short and long transport length CLHPs utilized neon as the working fluid and operated at a temperature range of 30-40K. Preliminary test results showed that the short and long transport length CLHPs were able to transport a heat load of 0.1-2.5W and 0.1-0.8 W respectively. Gully et al. [26] designed and experimentally studied a nitrogen-charged CLHP, where the effects of heat load, charged pressure and radiation heat load were studied in steady state operation, and a maximum heat load of 19W was achieved over a transport distance of 0.5m. All the CLHPs mentioned above employed a single-tube condenser where the flow resistance is relatively large. In order to reduce the flow resistance in the condenser and increase the heat transport capacity of CLHPs, Zhao et al. [27, 28] first proposed a nitrogen-charged CLHP with a parallel condenser design. Experimental results confirmed that the CLHP could operate with a high heat transfer capacity up to 41W across a 0.48m transport distance.

From the above review, it is clear that CLHP is an effective and efficient cryogenic heat transport device with many potential cryogenic applications. However, most current studies are still in the proof-of-concept stage, where proper design of the evaporator and condenser structures to satisfy the connection requirements with the heat source and heat sink has not been considered. At the same time, for space applications especially for the space infrared exploration system, a miniaturization design with reduced system volume/weight should be

conducted. Besides these aspects, high reliability and long life design is of high priority, because the design life of the next generation infrared observation satellites is over ten years or even longer, and on-orbit maintenance is generally impossible for most space missions. Although there is no moving parts in the CLHPs, which promises a long life nature, however, learning from the experience of applying ambient loop heat pipes in the spacecraft thermal control system, it is possible that the operation anomaly or failure may occur for the loop heat pipes under orbital conditions occasionally. For instance, for the spacecraft TacSat 4 launched in 2011, the Central Thermal Bus design of the thermal control system utilized an ambient loop heat pipe to acquire/transport waste heat from the on-board electronics and reject it to space via radiator panels. After a period of operation, operation anomaly occurred for the loop heat pipe, resulted in much degraded performance of the thermal control system [32]. Several years ago, operation anomaly also occurred for a loop heat pipe applied in the thermal control system of the Geoscience Laser Altimetry System on the ICESat Satellite [33]. Therefore, it is quite necessary to adopt the redundancy design to improve the operation reliability and realize a long life operation.

In order to address these issues and promote the future space applications of CLHPs , a CLHP-based thermal control system with redundancy design was proposed in this work, where a miniature nitrogen-charged CLHP was designed and fabricated considering appropriate interfaces with the heat source and heat sink, i.e., a saddle design was used to realize easy connection between the cylindrical evaporator and simulated infrared detector, and a novel cylindrical condenser design provided convenient interface with the cold finger of a pulse tube refrigerator. To the best of our knowledge, this is the first experimental study on the CLHPs with redundancy design, and here we mainly focus on the supercritical startup process, which is a very complicated but indispensable process prior to the attainment of normal operation for CLHPs. Different working modes for the supercritical startup have been defined due to the adoption of redundancy design, and extensive experimental studies were conducted, as described in detail below.

2 Experimental setup

Fig. 1 shows the schematic view of the experimental rig in this work, which was comprised of two CLHPs, a heating system, a cryogenic cooling system, a temperature measurement and data acquisition system and a thermal-vacuum chamber. Fig. 2 shows the CLHP-based thermal control system with redundancy design where the two CLHPs (#1 and #2) were connected with a pulse tube refrigerator respectively, and Fig. 3 shows the photo of the CLHPs in the experiment. Because the CLHPs both employed an auxiliary loop to help realize the supercritical startup, it was composed of a main loop and a secondary loop in addition to a gas reservoir. The main loop included a primary evaporator, a primary CC (compensation chamber), a primary condenser and primary vapor and liquid lines. The secondary loop consisted of a secondary evaporator, a secondary CC, a secondary condenser and secondary loop lines. The gas reservoir with a comparatively large volume was utilized to reduce the system pressure at ambient state, and it was connected to the inlet of the primary condenser. All the components of the CLHP were made of stainless steel except that the primary and secondary evaporator wicks were made of sintered nickel powders. The operating temperature of the CLHPs was designed in the range of 80-100 K, and nitrogen whose purity was greater than 99.9995% was charged as the working fluid. Table 1 presents the basic parameters of the CLHPs, where CC represents the compensation chamber and OD and ID represent the outer and inner diameters respectively.

To realize the redundancy design, the primary evaporators of the two CLHPs were coupled to a copper saddle, as shown in Fig. 4, and a thin-film electric resistance heater was directly attached to the copper plate to simulate the heat generated from a space infrared detector. The heat load of the electric heater can be adjusted from 0 to 30W by altering the DC power output voltage with an uncertainty of ±5.0%, which can be transferred to both primary evaporators through the copper saddle. In addition, the two secondary evaporators of the CLHPs were both attached by a thin-film electric resistance heater respectively to provide auxiliary heat loads during the

supercritical startup. Two pulse tube refrigerators were employed as the cryogenic heat sink, whose cold fingers were connected with the two cylindrical primary condensers of the CLHPs respectively. The pulse tube refrigerator is a refrigeration device based on the Simon expansion principle to obtain the cooling effect through charging and discharging high purity helium gas in the pulse tube. It was composed of a cold finger, a compressor and a controller, with a cooling capacity greater than 4W at 70K. The pulse tube cold finger and the compressor made up the main body, and the controller modulate the input power for its operation. In the operation, the compressor can produce continuous sinusoidal pressure fluctuations, and the refrigerant gas experiences endothermic expansion at the low temperature side and exothermic compression at the high temperature side, to achieve the cooling effect through the phase modulation mechanism.

To reduce the parasitic heat load from the ambient surroundings, the CLHPs were placed in a thermal-vacuum chamber, and all the components except the gas reservoir were covered with multilayer insulation materials. As the pressure in the thermal-vacuum chamber can be maintained always below 1×10^{-3} Pa, the parasitic heat load by convective heat transfer becomes very small and can be safely neglected. Calibrated Type T thermocouples (TCs) with measuring uncertainties of ±1.0 K were used to monitor the temperature variations of some characteristic points along the loop, as shown in Fig. 5. To reduce the influence of gravity, the primary evaporator and the primary condenser of the two CLHPs were always placed in a horizontal plane in the experiments.

3 Definition of different working modes

For a CLHP-based thermal control system with a redundancy design, it is expected that there are four possible working modes: the normal working mode, the backup conversion mode, the malfunction conversion mode and the dual operation mode, which covers the system operation in the whole lifetime. In the normal working mode, only one CLHP with the connected pulse tube refrigerator is operating to provide cryocooling to the infrared detector, while the other one is in the idle state. The backup conversion mode means to start up the CLHP in the

idle state and shut down the other one in operation to realize a smooth switch of the operation between the two CLHPs, while maintaining the infrared detector at the normal working state. The malfunction conversion mode means when the pulse tube refrigerator in operation breaks down or other similar issues emerge, it is necessary to start up the other CLHP in the idle state to provide sufficient cryocooling. Under this condition, the infrared detector in operation must be first shut down before the completion of the supercritical startup of the other CLHP. At the end of the lifetime of the thermal control system, the cryocooling provided by a single one pulse tube refrigerator may be insufficient due to the performance degradation after several years of operation. Under such a condition, both CLHPs with their corresponding pulse tube refrigerators will be needed to operate simultaneously, so as to provide sufficient cryocooling, which is termed as the dual operation mode. This working mode is of great importance to guarantee the normal operation of the space infrared exploration system at the end of lifetime.

4 Experimental results and analysis

4.1 Normal working mode

Fig. 6(a) shows the temperature variations of some characteristic points along the loop during the supercritical startup of the #1 CLHP. As shown in Fig. 6(a), the supercritical startup was initiated from an initially supercritical temperature of about 300K. At 22 min, the cold finger of the pulse tube refrigerator began to take effect, and the temperatures at the secondary evaporator (TC10) and at the outlet of the primary condenser (TC7) dropped rapidly, due to direct contact with the cold finger of the refrigerator. At 50 min, the temperatures at the secondary evaporator, secondary evaporator outlet and primary condenser outlet dropped at a much faster rate, indicating that the temperatures of nitrogen gas in the primary condenser and secondary CC dropped to their saturation temperatures corresponding to the local pressure, and fluid condensation occurred there afterwards, making the heat transfer proceed in a more efficient way. Several minutes later, the temperatures at the secondary evaporator (TC10) and at the primary condenser outlet (TC7) began to drop slowly and remained at about 90 K, indicating

that nitrogen in the two-phase state began to exist there. As time went by, the inventory of liquid nitrogen in the secondary evaporator would increase gradually, and it would fully saturate the secondary evaporator wick eventually. At 60 min, a very large temperature drop occurred at the primary CC inlet (TC1) due to the arrival of the condensate from the primary condenser, from which it can be inferred that when the secondary CC was cooled, the temperature/pressure of the working fluid inside it dropped, and a fluid circulation from the gas reservoir through the primary condenser, primary liquid line and the secondary loop line to the secondary CC should exist, to continuously supply working fluid to the secondary CC.

With the temperature of the secondary evaporator remaining at 90 K for about 12 min, a heat load of 2.5W was applied to the secondary evaporator ($Q_{se}^{(1)}$), and no obvious temperature rise of the secondary evaporator (TC10) was observed, indicating that the secondary evaporator was started up successfully. Under such a condition, the secondary evaporator could act as a pump to drive the condensed liquid nitrogen in the primary condenser to the primary evaporator core and CC through the primary liquid line (path 1), as evidenced by continous temperature drop at the outlet of the primary CC (TC8), at the primary evaporator (TC3) and at the primary evaporator outlet (TC4). Note that, there was another flow path from the secondary evaporator to the primary evaporator core, i.e. from the secondary evaporator through the primary vapor line, primary evaporator vapor grooves and primary evaporator wick to the primary evaporator core (path 2). Because of the difference in flow resistance between the two paths from the secondary evaporator to the primary evaporator core, more than 80% of the heat load on the secondary evaporator would flow through the path 1. As the primary evaporator wick began to be saturated with liquid coming from the primary condenser, the capillary pressure developed by the primary evaporator wick would totally shut down path 2 and force all the heat load on the secondary evaporator to flow through the path 1, resulted in a more efficient cooling to the primary evaporator. This was evidenced by more rapid cooldown rate of the primary evaporator and a sudden temperature drop at the primary evaporator outlet (TC4) at about 150 min.

With the operation of the secondary evaporator for about 90 min, the primary evaporator temperature (TC3) dropped to about 90K and began to remain unchanged, indicating that nitrogen in the two-phase state began to exist in the primary evaporator wick. As time went by, the inventory of liquid nitrogen in the primary evaporator would increase gradually and fully saturate the primary evaporator wick eventually. With the primary evaporator temperature remaining at 90K for several minutes, a heat load of 1W was applied to the copper saddle (Q_{cs}), and the heat load applied to the secondary evaporator ($Q_{se}^{(1)}$) was reduced to 1W. No obvious temperature rise of the primary evaporator was observed, indicating that the primary evaporator was started up successfully. With the normal operation of the primary evaporator, the #1 CLHP realized the supercritical startup.

Fig. 6 (b) shows the temperature variations of some characteristic points along the loop during the supercritical startup of the #2 CLHP, which were similar to those of #1 CLHP during the whole supercritical startup process. However, in Fig. 6(b), the secondary evaporator had to operate for about 240 min with a heat load of 2.5W ($Q_{se}^{(2)}$) to realize the large temperature drop of the primary evaporator from the ambient state (300K) to the saturation temperature (90K), which became much longer than that of #1 CLHP (90 min). This phenomenon can be explained according to the difference in the structural size between the two CLHPs: because the inner diameter of the liquid line of #2 CLHP (1.0mm) is much smaller than that of #1 CLHP (2.0mm), the flow resistance in the liquid line of #2 CLHP becomes much larger. As discussed above, there are two paths from the secondary evaporator to the primary evaporator core, and only for path 1, the condensate in the primary condenser can be driven into the primary evaporator core with a much larger cryocooling capacity; at the same time, the cryocooling capacity is strongly dependent on the mass flowrate of the working fluid in path 1. For #2 CLHP, the considerably increased flow resistance in the primary liquid line changes the balance of the flow resistance between the two paths, which leads to much reduced mass flowrate in path 1, compared to the situation in #1 CLHP. Therefore a careful flow resistance analysis should be conducted in the CLHP design to effectively

accelerate the supercritical startup process.

4.2 Backup conversion mode

In the backup conversion mode, a smooth switch of the operation of the two primary evaporators will be completed while the infrared detector always keeps working, and the two pulse tube refrigerators have to be operating simultaneously for a period of time. Because the coefficient of performance (COP) of the pulse tube refrigerator is only 2.0% or even lower when it is operating at a cryogenic temperature range of 80-100K, it is a high energy-consuming component in the thermal control system. As the space power supply is limited, it is very important to accelerate the backup conversion by reducing the time of simultaneous operation of the two pulse tube refrigerators for the energy saving purpose.

4.2.1 Backup conversion without auxiliary operation

In order to reduce the backup conversion time maximally, backup conversion from #1 to #2 CLHP without an auxiliary operation of the secondary evaporator in advance was first experimentally studied, as shown in Fig. 7, where an operation failure occurred. At the initial state, the #1 CLHP was in normal operation with a heat load of 4W and 0.5W applied to the copper saddle and secondary evaporator respectively. At about 15 min, #2 pulse tube refrigerator was started, and the temperatures of the primary condenser (TC17) and secondary evaporator (TC21) of the #2 CLHP began to drop gradually. At about 70 min, the temperature of the secondary evaporator (TC21) of the #2 CLHP had dropped to the saturation temperature (90K) and remained at this value for several minutes, indicating that nitrogen in the two-phase state began to exist there and liquid nitrogen would saturate the secondary evaporator wick eventually. Then the #1 pulse tube refrigerator and heat load applied to the secondary evaporator of the #1 CLHP was turned off, and a heat load of 0.5W was applied to the secondary evaporator of the #2 CLHP simultaneously, trying to realize an instant switch of the operation of the two primary evaporators. The primary evaporator temperature of the #2 CLHP (TC14) began to rise continuously, indicating that an operation

failure occurred.

The reason for the operation failure was analyzed below. After the #1 CLHP with the connected #1 pulse tube refrigerator was totally shut down, a heat load of 4W and 0.5W was actually applied to the primary and secondary evaporators of the #2 CLHP respectively. Although the primary and secondary evaporator wicks of the #2 CLHP had been saturated by the liquid nitrogen, the working fluid in the primary liquid line was still in the vapor state with a relatively high temperature. With the circulation of the working fluid in the primary loop of the #2 CLHP, the nitrogen vapor in the primary liquid line was pushed into the primary evaporator core, thus causing insufficient liquid supply to the primary evaporator wick, and the normal operation would be interrupted accompanied by a continuous temperature rise of the primary evaporator of the #2 CLHP.

4.2.2 Backup conversion with auxiliary operation

In order to address the above issue and ensure a successful backup conversion, in the subsequent experiment, an auxiliary operation of the secondary evaporator of the #2 CLHP with a heat load of 2.5W was first implemented before the total shut down of the #1 CLHP with the connected #1 pulse tube refrigerator, to guarantee that the primary liquid line of the #2 CLHP was filled with liquid nitrogen prior to the startup of the primary evaporator.

As shown in Fig. 8, after the secondary evaporator wick of the #2 CLHP was fully saturated by the liquid nitrogen, different from the case in Fig. 7, a heat load of 2.5W was first applied to the secondary evaporator to start up the secondary loop, before the total shut down of the #1 CLHP with the #1 pulse tube refrigerator, With the circulation of the working fluid in the secondary loop of the #2 CLHP for about 10 minutes, the primary liquid line would be filled with liquid nitrogen, under such a condition, it was ready to start up the primary loop of the #2 CLHP. At about 102 min, the #1 pulse tube refrigerator and heat load applied to the secondary evaporator of the #1 CLHP was turned off, and a reduced heat load of 0.5W was applied to the secondary evaporator of the #2 CLHP simultaneously, to realize a switch of the operation of the two primary evaporators. It was as expected that

no obvious temperature rise of the primary evaporator of the #2 CLHP (TC14) was observed, indicating that a successful backup conversion was achieved.

In the backup conversion mode, because the primary evaporator of the backup CLHP has already been filled with liquid nitrogen, the purpose for the auxiliary operation of the secondary evaporator is only to make the primary liquid line flooded by the liquid nitrogen, and the time needed for the auxiliary operation of the secondary evaporator is remarkably reduced compared with the case in the normal working mode.

4.3 Malfunction conversion mode

Fig. 9 shows the temperature variations of some characteristic points along the loop during the supercritical startup in the malfunction conversion mode. At the initial state, the #2 CLHP was in the normal operation with a heat load of 4W and 0.5W applied to the copper saddle and secondary evaporator respectively. At 25 min, #2 pulse tube refrigerator was shut down to simulate the operation failure in real applications. Several minutes later, a sudden temperature drop occurred at the outlet of the primary evaporator of the #1 CLHP, indicating that a certain amount of heat load applied to the copper saddle was transferred to the primary evaporator of the #1 CLHP where vapor was generated and flowed out of the primary evaporator. At 30 min, it was found that the primary evaporator temperature of the #2 CLHP (TC14) rose quickly, indicating that an operation failure occurred for the thermal control system, then the heat load applied to the copper saddle was turned off, and the #1 pulse tube refrigerator was started to initiate a malfunction conversion.

As shown in Fig. 9, the supercritical startup process of the #1 CLHP is similar to that in Fig. 6(a); however, the time needed for the auxiliary operation of the secondary evaporator was reduced remarkably, i.e., in Fig. 6(a), the secondary evaporator had to operate for about 90 minutes to realize the cryocooling to the primary evaporator, while here only 40 minutes was needed, that was because the primary evaporator of the backup CLHP (#1 CLHP) was always in a cryogenic state, and the cryocooling needed to realize the liquid saturation of the primary

293 evaporator wick decreased considerably. In the malfunction conversion mode, the simulated infrared detector had
294 to be shut down for about 120 minutes.

295 **4.4 Dual operation mode**

296 Fig. 10 shows the temperature variations of some characteristic points along the loop during the supercritical
297 startup of the two CLHPs. As shown in Fig. 10, at the initial state, all the characteristic points along the loop were
298 at the ambient temperature of about 295 K, and the supercritical startup of the two CLHPs was initiated
299 simultaneously. After the secondary evaporator wicks of the two CLHPs were fully saturated by the liquid, a heat
300 load of 2.5W was applied to the secondary evaporators of the two CLHPs respectively to start up the secondary
301 loop. After the primary evaporator wicks of the two CLHPs were fully saturated by the liquid, a heat load of 4W
302 was applied to the copper saddle, and the heat loads applied to the secondary evaporators were both reduced to 1W.
303 No obvious temperature rise of each primary evaporator was observed, indicating that the normal operation for
304 each CLHP was established, and successful supercritical startup of the two CLHPs in dual operation mode was
305 achieved. During the supercritical startup, it took about 120 minutes for the auxiliary operation of the secondary
306 evaporators to realize the cryocooling to the two primary evaporators from an ambient temperature (295K) to their
307 saturation temperature (90K), which was between the times required by #1 and #2 CLHPs in the normal working
308 mode, i.e., 90 and 240 minutes respectively, indicating that heat transfer between the #1 and #2 primary
309 evaporators through the copper block should exist to help the #2 primary evaporator to accelerate the temperature
310 drop process.

311 In the dual operation mode, obvious temperature oscillation phenomenon was observed for the #1CLHP when
312 the heat load applied to the secondary evaporator was relatively small. As shown in Fig. 11, when the heat load
313 applied to the secondary evaporator of the #1CLHP was 1W, obvious temperature oscillation at the inlets of the
314 primary CC (TC1) and the primary condenser (TC5) was observed; however, when the heat load applied to the

315 secondary evaporator was increased to 1.5W, the temperature oscillation phenomenon would disappear completely.
316 This phenomenon may be explained as follows: when the heat load applied to the secondary evaporator is
317 relatively small, the total mass flowrate in the primary liquid line was small accordingly, and the return subcooling
318 may be insufficient to offset the heat leak to the primary CC from both the primary evaporator and the ambient
319 surroundings, causing an increase of the temperature/pressure in the primary CC and resultant oscillation
320 movement of the working fluid along the main loop; however, when the heat load applied to the secondary
321 evaporator is increased to appropriate relatively high level, the total mass flowrate in the primary liquid line
322 increases accordingly, and the return subcooling becomes sufficient to offset the heat leak to the primary CC,
323 under this condition, oscillation flow in the main loop will be completely impossible.

324 **5 Conclusions**

325 A CLHP-based thermal control system with redundancy design for future space infrared exploration system was
326 designed and fabricated, and an extensive experimental study on the supercritical startup characteristics under four
327 possible working modes was conducted, where the temperature variations of some characteristic points along the
328 loop were presented, and the mechanisms responsible for specific phenomenon were analyzed. According to the
329 experimental results, important conclusions have been reached as summarized as follows:

330 ◆ In the normal working mode, with 2.5W applied to the secondary evaporator, each CLHP could successfully
331 realize the supercritical startup independently; however, the required time differed a lot because the
332 difference in the transport line diameter significantly affected the cryocooling capacity to the primary
333 evaporator, and a smaller diameter transport line may result in a much longer supercritical startup time.

334 ◆ In the backup conversion mode, instant switch of the two primary evaporators may cause an operation failure,
335 and an auxiliary operation of the secondary evaporator of the backup CLHP in advance was necessary to
336 make the primary liquid line filled with liquid and ensure a successful backup conversion.

337 ◆ In the malfunction conversion mode, the simulated infrared detector had to be first shut down, but the time
338 needed for the backup CLHP to realize the supercritical startup become obviously shorter than that in the
339 normal working mode because the primary evaporator of the backup CLHP was always in a cryogenic state,
340 and the cryocooling needed to realize the liquid saturation of the primary evaporator wick decreased
341 considerably.
342 ◆ In the dual operation mode, the two CLHPs could realize the supercritical startup simultaneously, and the
343 time needed was between the ones required by the two CLHPs in the normal working mode, due to the heat
344 transfer between the two primary evaporators through the copper saddle; however, a temperature oscillation
345 phenomenon was observed, which can be eliminated effectively by increasing the heat loads applied to the
346 secondary evaporator.
347 As the first reported experimental study on a CLHP-based thermal control system with redundancy design, the
348 experimental results and analysis provided here contribute greatly to the design and future space applications of
349 such an advanced thermal control system with high reliability and long lifespan.
350 **Acknowledgement**
351 This work was supported by the National Natural Science Foundation of China (No. 51306009 and 51406009),
352 Beijing Natural Science Foundation (No.3144031), and the EU Marie Curie Actions-International Incoming
353 Fellowships (FP7-PEOPLE-2013-IIF-626576). The authors are very grateful to Li Guoguang and Li Lei in the
354 Beijing Institute of Spacecraft System Engineering, China Academy of Space Technology, for their help in the
355 preparation of the experiments.
356

References

[1] G.P. Peterson, An introduction to heat pipes, 1st ed. Singapore: John Wiley & Sons, Inc., 1994

[2] A. Faghri, Heat pipe science and technology, 1st ed. London: Taylor & Francis, Inc., 1995

[3] R.S. Gaugler, Heat transfer device, U.S. Patent No. 2350 348, 1944

[4] S. Hong, X. Zhang, Y. Tang, et al., Experiment research on the effect of the evaporator's configuration design of an innovative ultra-thin looped heat pipe, International Journal of Heat and Mass Transfer 92(2016) 497-506

[5] Y. F. Maydanik, Loop heat pipes, Applied Thermal Engineering 25 (2005) 635-657

[6] L. Bai, G. Lin, D. Wen, et al. Experimental investigation of startup behaviors of a dual compensation chamber loop heat pipe with insufficient fluid inventory, Applied Thermal Engineering 29 (2009)1447-1456

[7] T. Tharayil, L.G. Asirvatham, V. Ravindran, et al., Thermal performance of miniature loop heat pipe with graphene-water nanofluid, International Journal of Heat and Mass Transfer, 93(2016) 957-968

[8] Yuechao Deng, Zhenhua Quan，Yaohua Zhao，et al., Experimental research on the performance of household-type photovoltaic-thermal system based on micro-heat-pipe array in Beijing, Energy Conversion and Management 106(2015)1039-1047

[9] M.S. Naghavi, K.S. Ong, M. Mehrali, et al., A state-of-the-art review on hybrid heat pipe latent heat storage systems, Energy Conversion and Management 105(2015) 1178-1204

[10] H. Jafari Mosleh, S. Jahangiri Mamouri, M.B. Shafii, et al., A new desalination system using a combination of heat pipe, evacuated tube and parabolic trough collector, Energy Conversion and Management 99 (2015)141-150

[11] R. M. Fairuz, D. Abhijit, O. Bradley, et al., Experimental investigation of combined heat recovery and power generation using a heat pipe assisted thermoelectric generator system, Energy Conversion and Management, 111(2016) 147-157

[12] K. Nithyanandam and R. Pitchumani, Design of a latent thermal energy storage system with embedded heat pipes, Applied Energy 126(2014) 266-280

[13] Kai-Shing Yang, Tsung-Yi Yang, Cheng-Wei Tu, et al., A novel flat polymer heat pipe with thermal via for cooling electronic devices, Energy Conversion and Management 100 (2015) 37-44

[14] T.T. Hoang, T.A. O'Connell. Performance demonstration of flexible advanced loop heat pipe for across-gimbal cryocooling. AIAA paper, No.2005-5590, 2005

[15] T.T. Hoang, T.A. O'Connell, J. Ku, et al. Performance Demonstration of a Hydrogen Advanced Loop Heat Pipe for 20-30K Cryocooling of Far Infrared Sensors. Proceedings of SPIE 5904(2005) No.590410

[16] H. Pereira, F. Haug, P. Silva, et al, Cryogenic loop heat pipes for the cooling of small particle detectors at CERN, Advances in Cryogenic Engineering: Transactions of the Cryogenic Engineering Conference 55(2010) 1039-1046

[17] D. Khrustalev, S. Semenov, Advances in Low-Temperature, Cryogenic and Miniature Loop Heat Pipes, Presentation at the 12th Annual Spacecraft Thermal Control Technology Workshop, El Segundo, March 2003

[18] D. Khrustalev, Cryogenic Loop Heat Pipes as Flexible Thermal Links for Cryocoolers, Proc. of the 12th Int. Cryocooler Conference, June 18-20, 2002, Cambridge, MA, USA, pp. 709-716

[19] D. Khrustalev, Test Data for a Cryogenic Loop Heat Pipe Operating in the Temperature Range from 65k to 140K, Presentation at the International Two-Phase Thermal Control Technology Workshop, Mitcheville, MD, September 24-26, 2002

[20] Q. Mo, J. Liang. A novel design and experimental study of a cryogenic loop heat pipe with high heat transfer capability, International Journal of Heat and Mass Transfer 49(2006) 770-776

[21] Q. Mo, J. Liang, J. Cai. Investigation of the effects of three key parameters on the heat transfer capability of a CLHP, Cryogenics 47(2007) 262-266

[22] Q. Mo, J. Liang. Operational performance of a cryogenic loop heat pipe with insufficient working fluid inventory, International Journal of Refrigeration 29(2006) 519-527

[23] Y. James, E. Kroliczek，L. Crawford. Development of a Cryogenic Loop Heat Pipe (CLHP) for Passive Optical Bench

401 Cooling Applications. SAE paper, No. 2002-01-2507

402 [24] D. Bugby, B. Marland, C. Stouffer, et al., Across-gimbal and miniaturized cryogenic loop heat pipes, Space technology and
403 applications international forum-STAIF (2003) 218-226

404 [25] D. Bugby, B. Marland, C. Stouffer, et al., Development of advanced tools for cryogenic integration, Advances in Cryogenic
405 Engineering: Transactions of the Cryogenic Engineering Conference 49(2004) 1914-1922

406 [26] P. Gully, Q. Mo, T. Yan, et al. Thermal behavior of a cryogenic loop heat pipe for space application, Cryogenics 51 (2011)
407 420-428

408 [27] Y. Zhao, T. Yan, J. Liang, Experimental study on a cryogenic loop heat pipe with high heat capacity, International Journal of
409 Heat and Mass Transfer 54 (2011) 3304-3308

410 [28] T. Yan, Y. Zhao, J. Liang, et al., Investigation on optimal working fluid inventory of a cryogenic loop heat pipe, International
411 Journal of Heat and Mass Transfer 66 (2013) 334-337

412 [29] T.T. Hoang, T.A. O'Connell, J. Ku, et al., Large Area Cryocooling for Far Infrared Telescopes，Proceedings of SPIE Vol. 5172
413 (2003) 77-85

414 [30] T.T. Hoang, T.A. O'Connell, D.A. Suhkov, Large Area Cooling with Cryogenic Loop Heat Pipes, AIAA paper, No. 2007-4272,
415 2007

416 [31] L. Bai, L. Zhang, G. Lin, et al., Development of cryogenic loop heat pipes: A review and comparative analysis, Applied
417 Thermal Engineering 89(2015)180-191

418 [32] Hoang T.T., Armiger W.J., Baldauff R.W., et al. Performance of COMMx Loop Heat Pipe on TacSat 4 Spacecraft, AIAA paper,
419 No. 2012-3498, 2012

420 [33] Baker C., Butler D., Grob E., et al. Geoscience laser altimetry system (GLAS) loop heat pipe anomaly and on orbit testing,
421 AIAA paper, No. 2011-5209, 2011

422

Table captions:

Table1 Basic parameters of the tested CLHPs

Figure captions:

Fig. 1 A schematic view of the experimental system

Fig. 2 A schematic view of the CLHP-based thermal control system with redundancy design

Fig. 3 Photo of the two CLHPs in the experiment

Fig. 4 Detailed structure of the two primary evaporators coupled by a copper saddle

Fig. 5 Thermocouple locations along the loop of the two CLHPs

Fig. 6 Supercritical startup process of the two CLHPs in the normal working mode

Fig. 7 Supercritical startup process without auxiliary operation in the backup conversion mode

Fig. 8 Supercritical startup process with auxiliary operation in the backup conversion mode

Fig. 9 Supercritical startup process in the malfunction conversion mode

Fig. 10 Supercritical startup process in the dual operation mode

Fig. 11 Temperature oscillation phenomenon in the dual operation mode

Table1 Basic parameters of the tested CLHPs

Components		Dimensions	
		#1 CLHP	#2CLHP
Primary evaporator	Casing OD/ID ×length of /mm	13×11×50	13×11×50
	Wick OD/ID ×length/mm	11×4×40	11×4×40
Secondary evaporator	Casing OD/ID ×length/mm	35×13×11	35×13×11
	Wick OD/ID ×length/mm	11×4×27	11×4×27
Primary loop	Liquid line OD/ID ×length/mm	3×2×600	2×1×600
	Condenser line OD/ID ×length/mm	2×1×700	2×1×700
	Vapor line OD/ID ×length/mm	3×2×700	3×2×700
Secondaryloop	Liquid line OD/ID ×length/mm	3×2×700	2×1×700
	Condenser line OD/ID ×length/mm	2×1×260	2×1×260
	Vapor line OD/ID ×length/mm	3×2×30	3×2×30
Wick	Maximum capillary radius/μm	0.5	0.5
	Porosity	55%	55%
	Permeability/m^2	$>7\times10^{-14}$	$>7\times10^{-14}$
Gas reservoir	Volume/ml	500	475

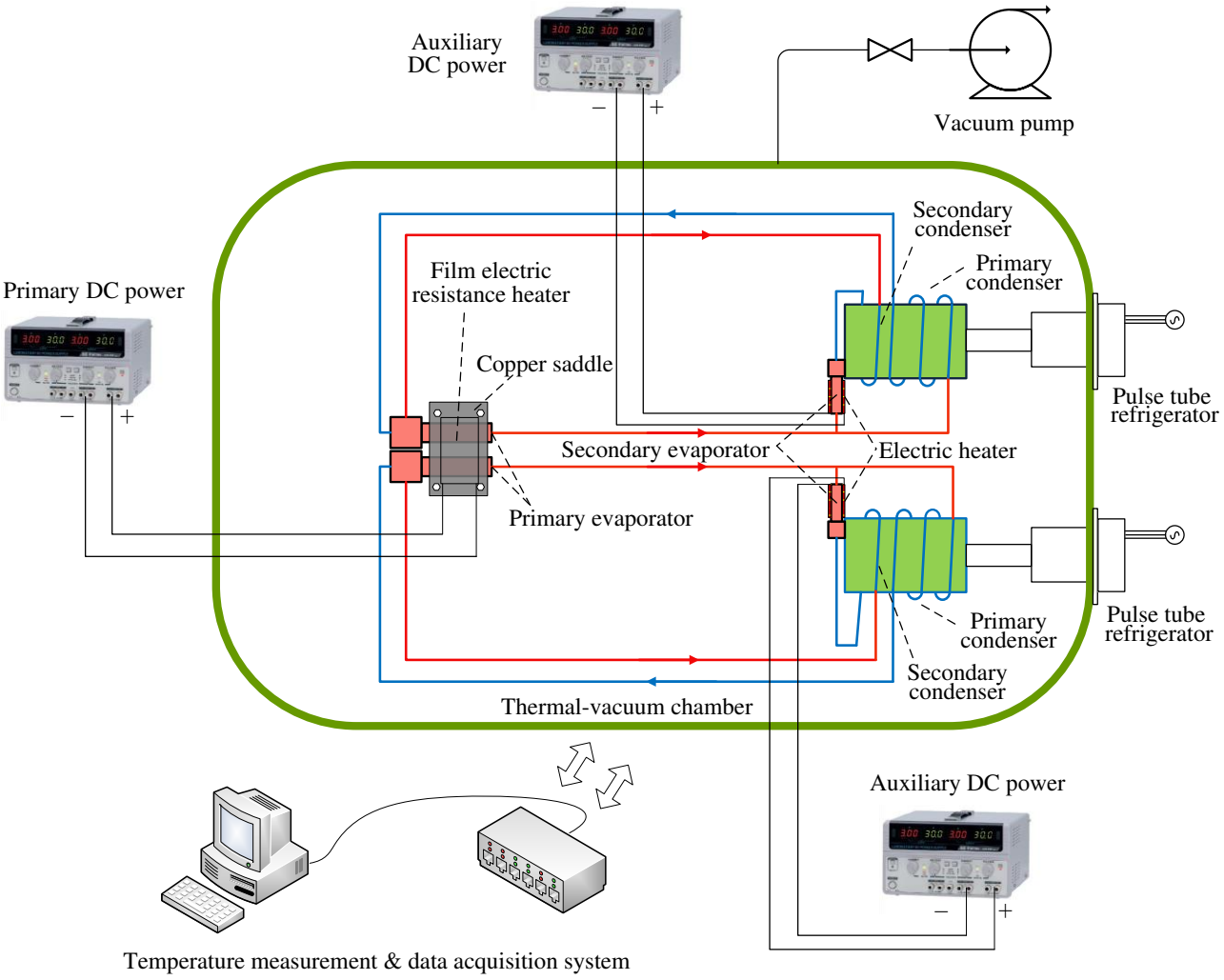

Fig. 1 A schematic view of the experimental system

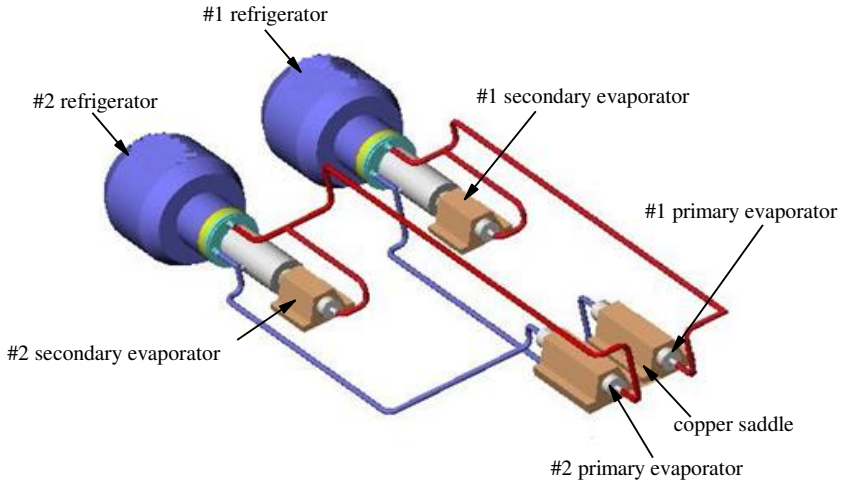

Fig. 2 A schematic view of the CLHP-based thermal control system with redundancy design

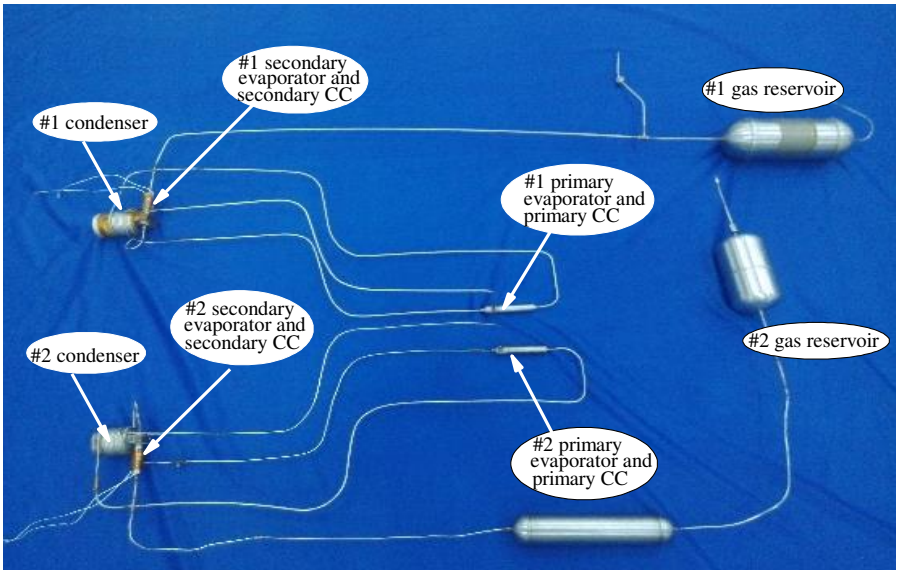

Fig. 3 Photo of the two CLHPs in the experiment

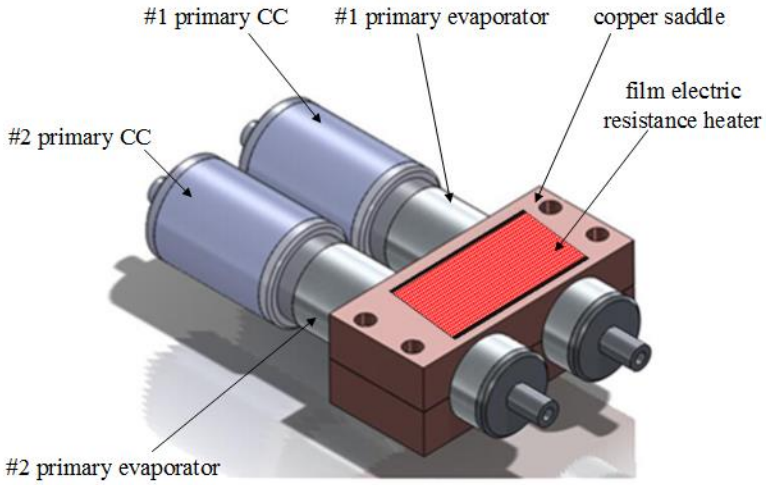

Fig. 4 Detailed structure of the two primary evaporators coupled by a copper saddle

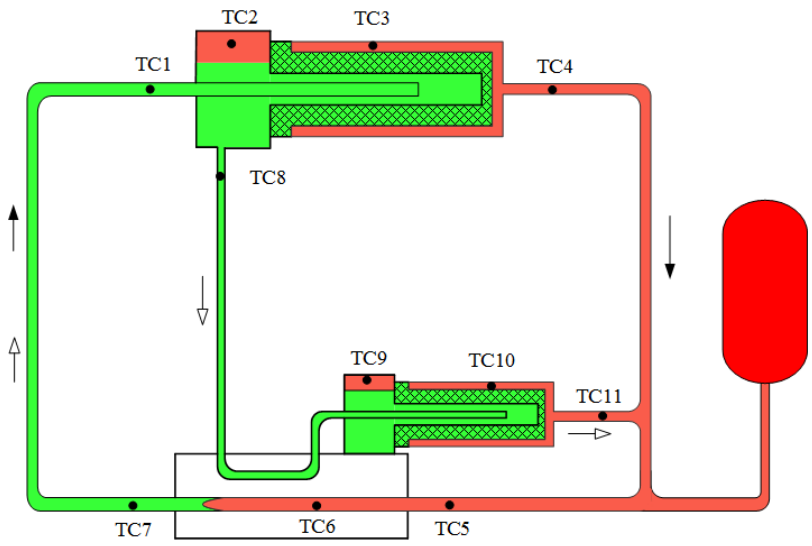

(a) #1 cryogenic loop heat pipe

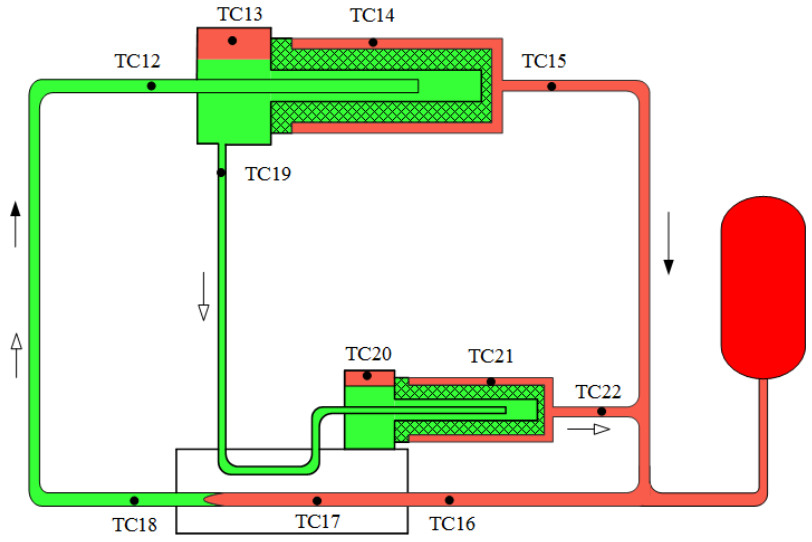

(b) #2 cryogenic loop heat pipe

Fig. 5 Thermocouple locations along the loop of the two CLHPs

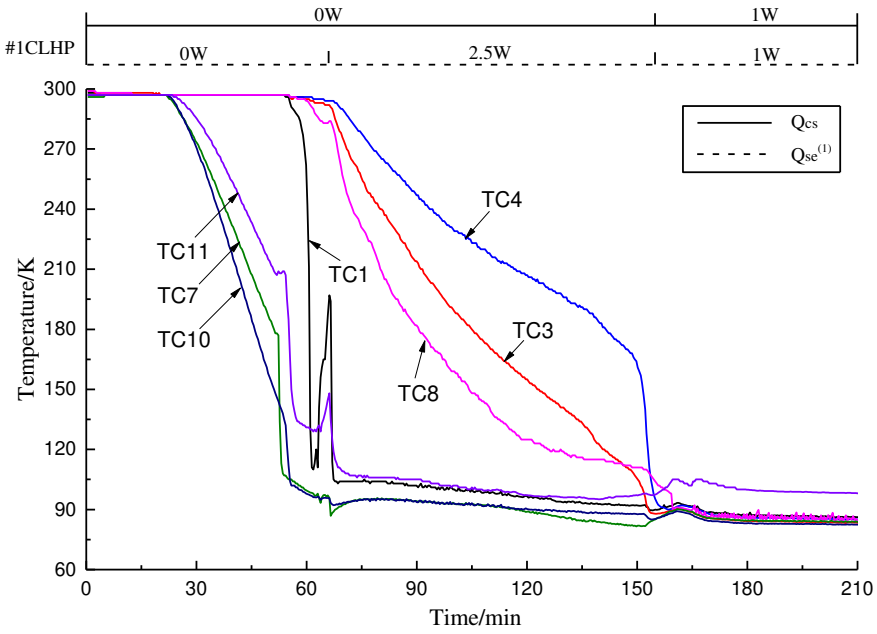

(a) #1 cryogenic loop heat pipe

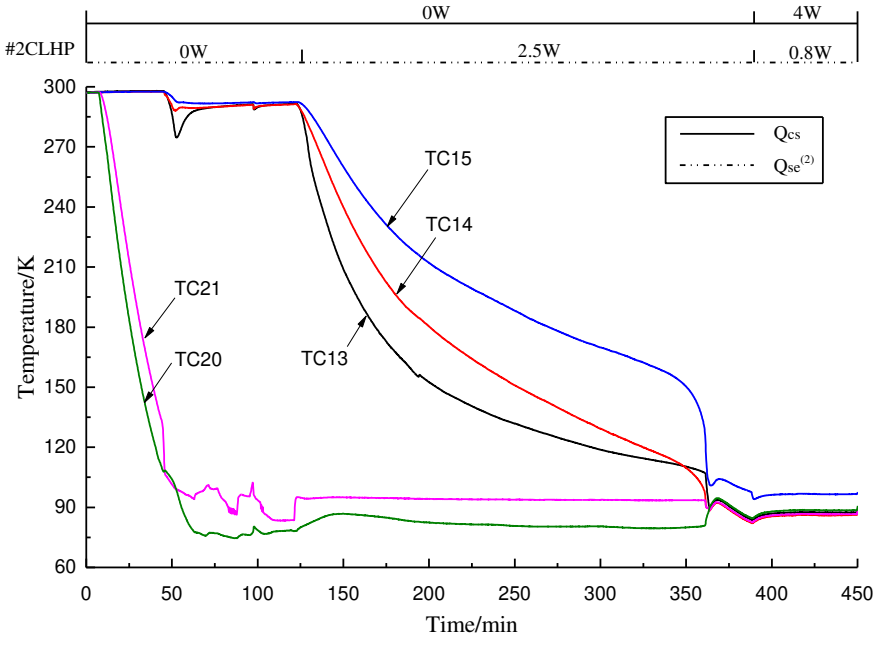

(b) #2 cryogenic loop heat pipe

Fig.6 Supercritical startup process of the two CLHPs in the normal working mode

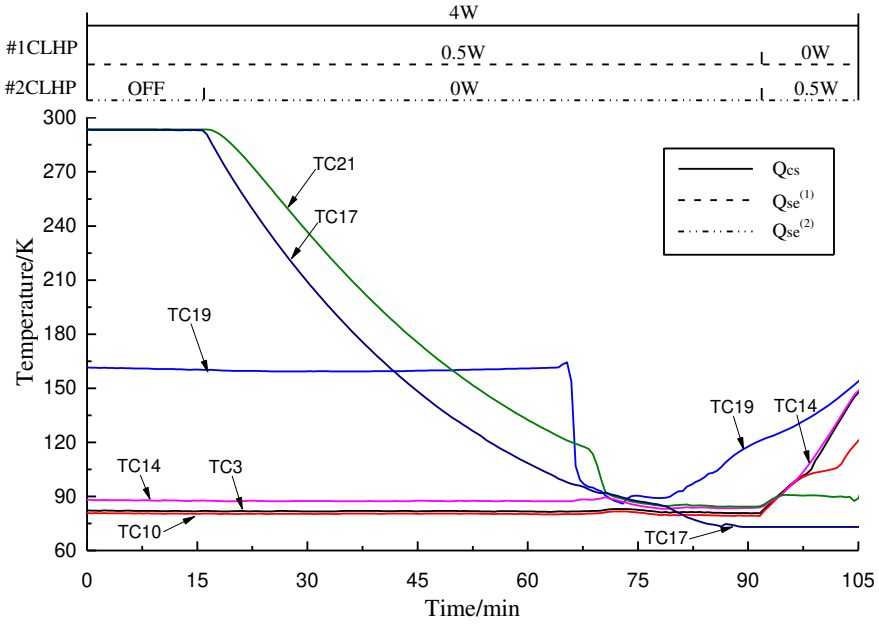

(a) the whole range

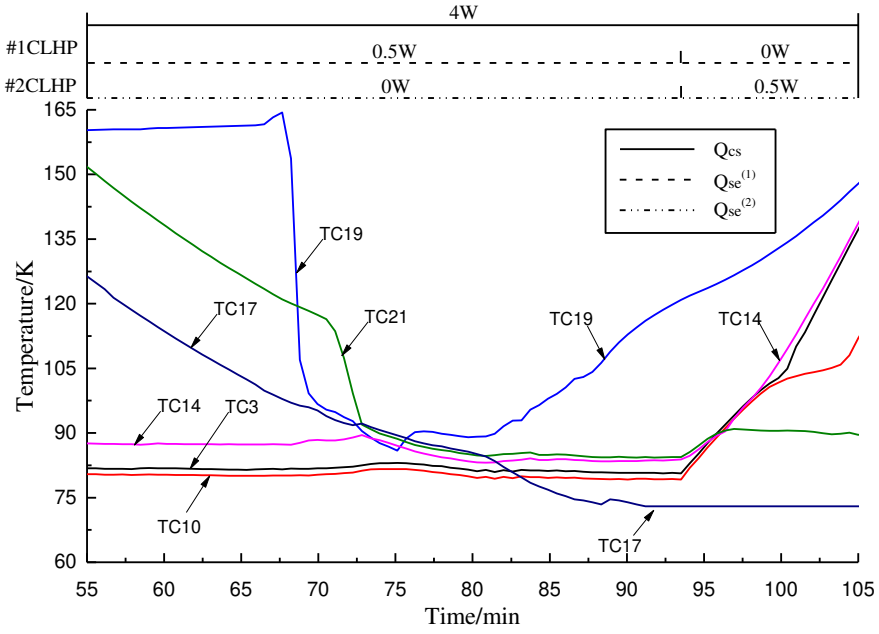

(b) local enlargement

Fig. 7 Supercritical startup process without auxiliary operation in the backup conversion mode

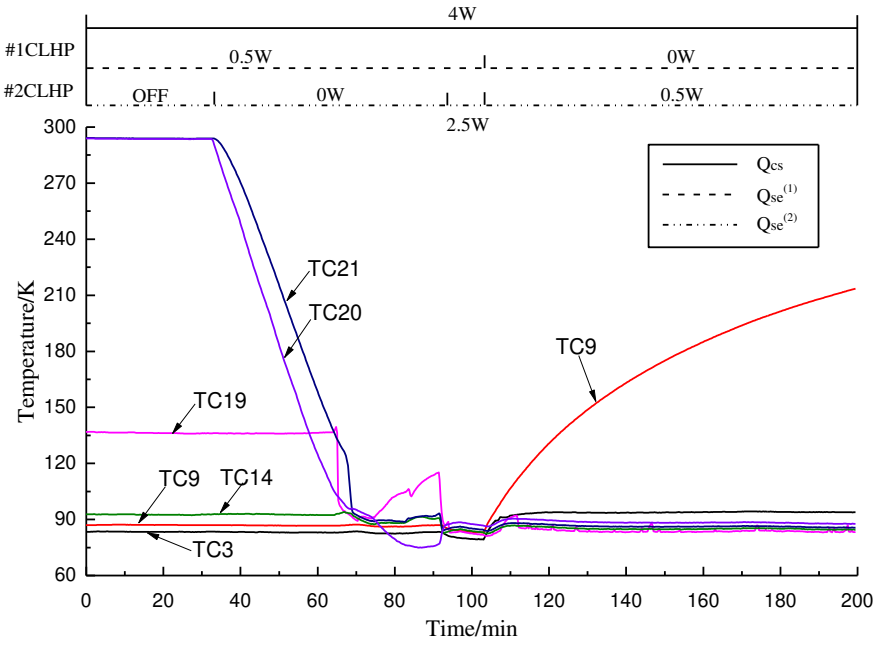

(a) the whole range

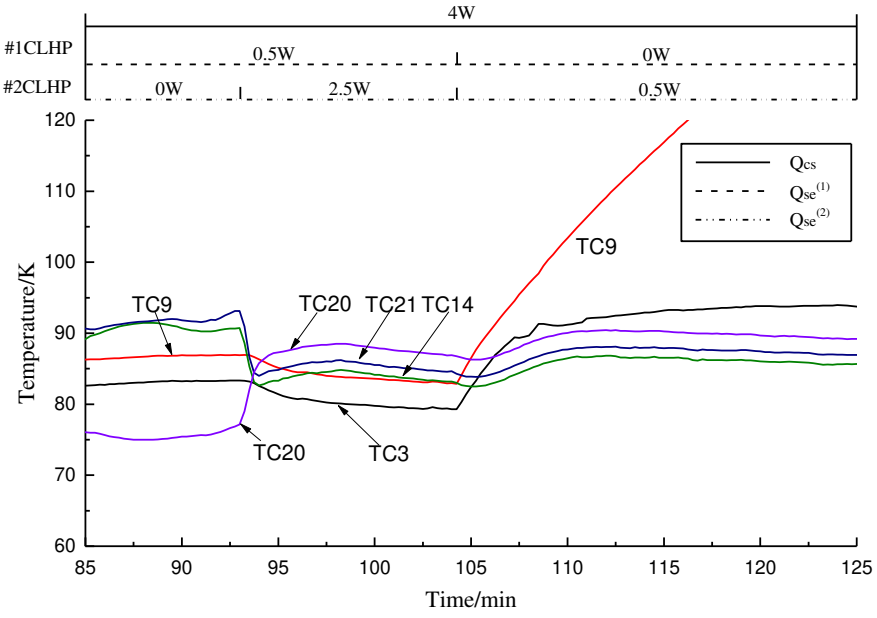

(b) local enlargement

Fig. 8 Supercritical startup process with auxiliary operation in the backup conversion mode

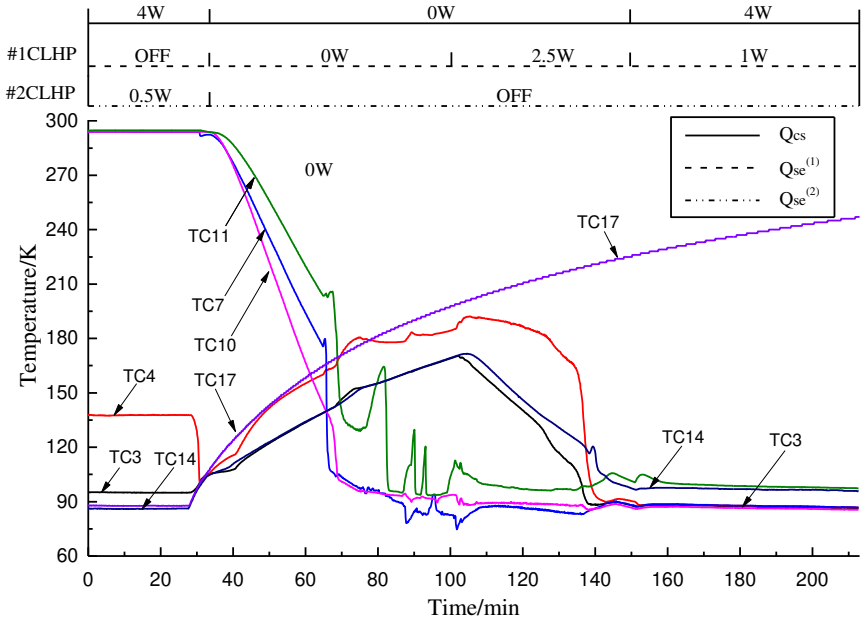

Fig. 9 Supercritical startup process in the malfunction conversion mode

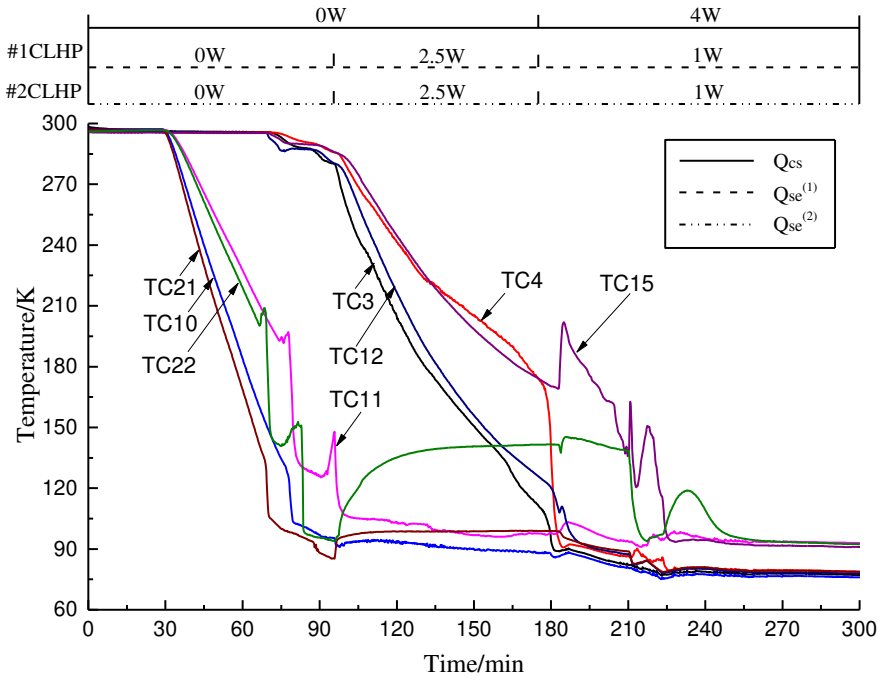

Fig. 10 Supercritical startup process in the dual operation mode

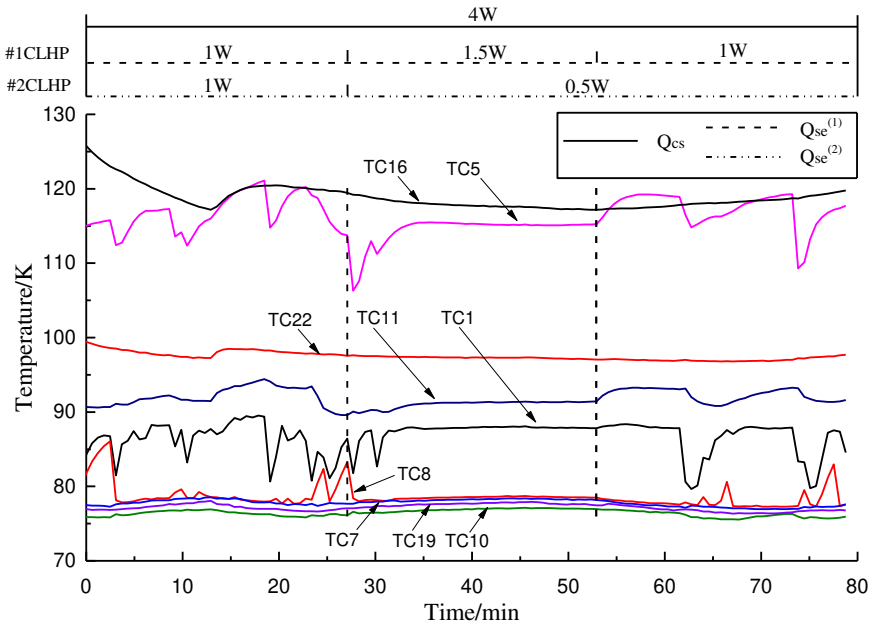

Fig.11 Temperature oscillation phenomenon in the dual operation mode